

Electronic Supplementary Information for the article

Spin mixing at level anti-crossings in the rotating frame makes high-field SABRE feasible

Andrey N. Pravdivtsev,^{a,b} Alexandra V. Yurkovskaya,^{a,b} Hans-Martin Vieth,^c and Konstantin L. Ivanov^{a,b}

^a International Tomography Center, Siberian Branch of the Russian Academy of Science, Institutskaya 3a, Novosibirsk, 630090, Russia. E-mail: ivanov@tomo.nsc.ru; Tel.: +7(383)330-8868; Fax: +7(383)333-1399

^b Novosibirsk State University, Pirogova 2, Novosibirsk, 630090, Russia.

^c Institut für Experimentalphysik, Freie Universität Berlin, Arnimallee 14, Berlin, 14195, Germany.

This file contains details of sample preparation; calculation algorithm; results for Crabtree' catalyst and other substrates; NMR parameters of the spin systems.

I. Experimental methods

In experiments with pyridine two different samples were used. Sample 1 contained 3.3 μl of pyridine (py) and 1 mg of the IrMesCODCl pre-catalyst in 650 μl of MeOD. Sample 2 contained 3.3 μl of py and 1 mg of Crabtree's catalyst in 650 μl MeOD. In experiments with other substrates we always used the IrMesCODCl pre-catalyst and prepared the following samples: 20 mM of 4,4'-bipyridine and 4 mM of IrMesCODCl in 650 μl MeOD; 6 mM of 2,2'-bipyrazine and 4 mM of IrMesCODCl in 500 μl MeOD and 100 μl DMSO; 60 mM of 3-methyl-1H-pyrazole and 4 mM of IrMesCODCl in 600 μl MeOD.

Experiments were run at a 200 MHz NMR spectrometer. To observe the high-field SABRE effects we used a protocol with the following stages. **Stage 1:** waiting period of a duration of 20 s required for the spins to relax to thermal equilibrium. **Stage 2:** bubbling the parahydrogen gas through the solution for 6 s. **Stage 3:** waiting for 1.5 s in order to get rid of the gas bubbles in the sample. **Stage 4:** applying RF-irradiation for a period τ_{rf} of variable duration in the range 0.1-7 s. **Stage 5:** detection of the transverse magnetization formed due to the high-field SABRE effect immediately after switching off the RF-field (i.e., without applying any detecting pulses). Experiments were carried out at three different RF-field amplitudes equal to 28.6 kHz, 20.3 kHz and 11.4 kHz for the two catalysts and py as a substrate. In order to optimize the enhancement for dihydrogen, which has shorter relaxation time as compared to py, we used shorter duration of the spin-locking period, which was $\tau_{rf}=0.7$ s.

NMR enhancement factors were measured in the following way. Thermal polarization values were obtained from NMR spectra measured prior to bubbling the sample by parahydrogen. Then signals of substrates in RF-SABRE were divided by their thermal signals giving signal enhancement.

To obtain the enhancement factor for dihydrogen in the solvent bulk and at the active complex we ran the SABRE experiments as described above, introduced a sufficiently long waiting period in order to let the spins relax to equilibrium and then acquired a thermal NMR spectrum. It was possible to measure thermal signal intensities for dihydrogen after four acquisitions. After that, the enhancement factor for dihydrogen was obtained as the ratio of the signals in the RF-SABRE spectrum and in the thermal NMR spectrum.

Hereafter we will also use the following abbreviations for different compounds: aPy-axial py, ePy-equatorial py in the complex; fPy=free py in the solution; H₂ is dihydrogen in the solvent bulk, c-H₂ is dihydrogen at the active complex.

II. Calculation method

To model the SABRE effect on the quantitative level we used a theoretical approach, similar to the one used earlier^{1,2}. We described polarization transfer in a system, which consists of 2 spins of parahydrogen and 5 protons of py; in the case of Crabtree's catalyst also the spin of the ³¹P nucleus was included in the calculation. The spin system at high magnetic field B_0 in the presence of the RF-field is

described by the following Hamiltonian in the rotating reference frame:

$$\hat{H}_{rf} = - \sum_{\alpha=1}^7 (v_{\alpha} - v_{rf}) \hat{I}_{\alpha z} + \sum_{\alpha \neq \beta}^7 J_{\alpha\beta} (\hat{\mathbf{I}}_{\alpha} \cdot \hat{\mathbf{I}}_{\beta}) - v_1 \sum_{\alpha=1}^7 \hat{I}_{\alpha x} - v_p \hat{F}_z + \sum_{\alpha=1}^7 J_{\alpha P} \hat{I}_{\alpha z} \hat{F}_z$$

Here spin operators of the α -th protons are denoted as $\hat{I}_{\alpha x, y, z}$; \hat{F}_z defines the z-projection of the ³¹P spin. The NMR frequencies of protons, v_{α} , are given by their chemical shifts, δ_{α} , and the proton gyromagnetic ratio, γ_p : $v_{\alpha} = (1 + \delta_{\alpha})\gamma_p B_0 / 2\pi$. The NMR frequency, v_p , of the phosphorus nucleus is very different from those of the protons; for this reason for ³¹P only the z-operator of spin is important. Proton-proton scalar couplings are denoted by $J_{\alpha\beta}$; proton-phosphorus couplings are denoted as $J_{\alpha P}$. All the NMR parameters were determined from the NMR spectra; their values are given in Table 1S for both complexes. For spectral assignment we used high resolution 1D NMR spectra and 2D TOCSY spectra.

To describe the resulting spin order we calculated the density matrix of the spin system. As initial condition we have taken the density matrix, ρ_{in} , which describes the singlet-state preparation of the protons originating from parahydrogen and zero polarization for all the other spins. After that, this matrix was evaluated in the eigen-basis of the Hamiltonian \hat{H}_{rf} ; in this matrix we removed all off-diagonal elements and obtained the resulting density matrix, ρ_{fin} . The removed elements describe spin coherences, which are washed out due to the long period of preparation of polarization. Then, using this new matrix, spin magnetizations, M_{ax} and M_{ay} , were calculated as the expectation values of the corresponding spin operators:

$$M_{ax} = \text{Tr}\{\hat{I}_{ax}\rho_{fin}\}, \quad M_{ay} = \text{Tr}\{\hat{I}_{ay}\rho_{fin}\}$$

This calculation scheme is known to be reasonably fast and precise to describe polarization transfer effects in PHIP and SABRE.

In the resulting RF-SABRE dependences on the RF-field parameters, v_{rf} and v_1 , in the case of multispin systems (e.g., protonated py) there are noise-like contributions, which arise from the large number of LACs in the coupled multi-spin system under study. Such noise-like features are irrelevant for the comparison with the experiment; furthermore, they disappear when inhomogeneity of the B₁-field is taken into account. For this reason, we performed calculations assuming spatially non-uniform B₁-field, i.e., averaged the result over a realistic distribution over the v_1 values. After this, the RF-SABRE dependences become smooth. Since signal amplitudes in the theory and in experiment are related arbitrarily, for a better comparison we also normalized the theoretical curves to the corresponding experimental ones, keeping a common scaling factor for the py protons.

III. LACs in the doubly tilted frame

In the main text we discussed the positions of LACs in the simplest system of an AA'M-type. This is indeed the

minimal system, which can be discussed in the context of SABRE as it treats the substrate with only one proton. However, there is still the question whether the results for the AA'M-system also apply to systems with more coupled protons. To answer this question, let us analyze the LACs in the case where the substrate has two 'isochronous' protons with identical chemical shift, so that the resulting spin system is of the AA'MM'-kind. We will also assume that the strongest coupling in the system is that between the two protons originating from parahydrogen, *i.e.*, the AA'-coupling. In this situation, in the Hamiltonian, \hat{H}_{rf} , the AA'- and MM'-couplings can be included in the main Hamiltonian, whereas the four AM-couplings are treated as a perturbative part, \hat{V} . Then the AA'-spins and MM'-spins can be quantized along their effective fields in the rotating frame, *i.e.*, the description based on the DTF is valid. This allows us to use the literature results to find the positions of LACs in the DTF²⁻⁴:

$$\pm(v_{A,dtf} - v_{M,dtf}) = J_{AA'} - J_{MM'}$$

crossing of $|ST_{\pm}\rangle_{dtf}$ and $|T_{\pm}S\rangle_{dtf}$

$$\pm(v_{A,dtf} - v_{M,dtf}) = J_{AA'} + J_{MM'}$$

crossing of $|SS\rangle_{dtf}$ and $|T_{\pm}T_{\mp}\rangle_{dtf}$

Thus, it is seen that the number of LACs has doubled as compared to the AA'M case. However, when $J_{AA'} \gg J_{MM'}$ the LACs are grouped in two pairs with almost the same positions. Effectively, each pair of LACs works as one LAC; its position as well as the resulting phase of the RF-SABRE polarization is nearly the same as for the AA'M-case. It is typical, that the AA'-coupling is large (about -7 Hz), whereas the coupling between the protons of the substrate is smaller; for instance, between the two ortho-protons of py it is below 1 Hz. For this reason, the relatively simple three-spin model given in the main text gives a valid quantitative description of the problem. When there are more spins in the system and the relation between them is arbitrary the LACs can only be identified from quantum-mechanical calculations. This is exactly the approach that we used to model the data.

IV. Experimental results

Here we will discuss further details of the dependence of the high-field SABRE effect on the two key parameters, RF-field frequency and strength. We will present the results for protonated py obtained with both catalysts and also the results for other substrates. Polarization of H₂ and *c*-H₂ will also be discussed.

A. Results for the complex with the IrMes catalyst

Typical RF-SABRE spectra of protonated py are shown in Figure 1S: one can readily see that for observing the effect it is crucial to set carefully the RF-field frequency.

The full frequency dependence is shown in Figure 2S. At any RF-field strength the frequency dependence contains positive and negative peaks, originating from the characteristic LACs in the spin system. It is clearly seen that the effect grows as ν_1 increases while the LAC region becomes broader (it is easier to fulfill the LAC conditions). The frequency dependences are in very good agreement

with the calculation; the same holds for the other protons, namely, the meta-protons of py, H₂ and *c*-H₂. Analogous results are seen for RF-SABRE obtained with Crabtree's catalyst (see below).

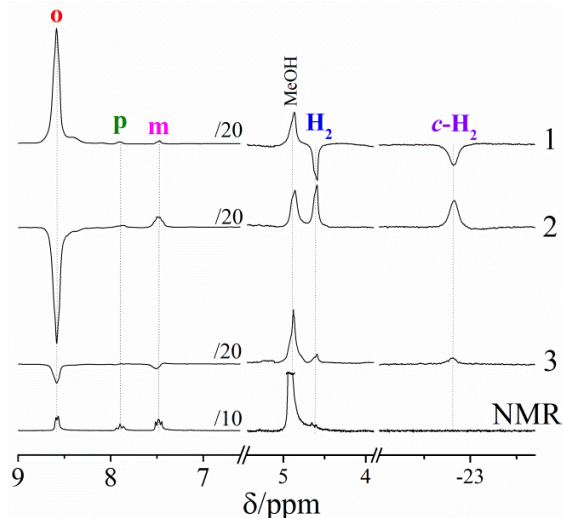


Figure 1S. ¹H RF-SABRE spectra obtained with the IrMes catalyst after applying an RF-field with amplitude of 28.6 kHz and frequency positions $\nu_{rf} = -7.0$ ppm (curve 1), -7.4 ppm (curve 2), and -7.9 ppm (curve 3). Positions of different protons are assigned. Letters *o, p, m* denote the ortho, para and meta-protons of py; H₂ and *c*-H₂ denote dihydrogen in the bulk and at the catalyst. The thermal single-scan NMR spectrum is also shown for comparison (bottom trace).

As has been mentioned in the main text, the achieved polarization amplitude is considerably larger than that at thermal equilibrium but is still smaller than that found for the SABRE effect at low fields. We attribute this decrease in polarization as compared to the low-field case to association-dissociation processes occurring during the spin-locking period. Since the chemical shifts of all protons are different at the complex and in the solution these chemical exchange processes result in modulation of $v_{A,dtf}$ and $v_{M,dtf}$ and also of the direction of the tilt axes. This causes variation of the RF-irradiation conditions, which tends to reduce polarization. When SABRE is done at low field this effect is not pronounced because all spins are then quantized along a fixed axis given by the direction of the external magnetic field. To reduce the unwanted effect at high field it is desirable to use strong RF-fields such that the DTF quantization axes almost coincide with the x-axis of the rotating frame for both free and catalyst-bound substrate. Our results clearly show that when ν_1 increases polarization grows in accordance with this expectation; however, with the field strengths available we were unable to reach the condition $\nu_1 \gg |\delta v_A|, |\delta v_M|$. Polarization of H₂ should be even more sensitive to the modulation effect because of the very large difference in the chemical shift of H₂ bound to catalyst (-22.8 ppm) and in solution (4.6 ppm). For this reason, and also because of fast relaxation of H₂ and the fact that some amount of H₂ goes to the gas phase the absolute signal intensity for H₂ is much smaller than for

the py protons but is still substantial, see below. For py the relaxation time is longer and the difference in chemical shift between the free and bound states is smaller, therefore high absolute signal intensities are achievable.

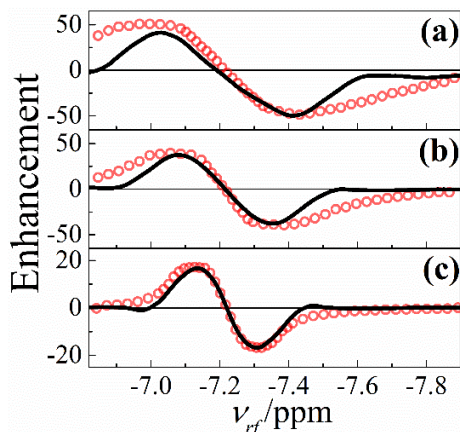


Figure 2S. Dependence of the RF-SABRE-induced NMR enhancement on ν_{rf} for different ν_1 values for the ortho-protons of free py: 28.6 kHz (a), 20.3 kHz (b) and 11.4 kHz (c). The RF-SABRE effect was observed for the IrIMes catalyst and the 2,6-protons of pyridine; lines show the simulation results.

Whereas in Figure 2S the results are shown only for the ortho-protons of py; it is also of interest to discuss the SABRE effects found for other enhanced signals in the spectra. These results are shown in Figure 3S and 4S. The highest enhancement is always observed for the ortho-protons; however, other protons (namely, the meta-protons of py, H_2 and $c-H_2$) are also polarized. Here it is important to mention that the opposite phase of H_2 and $c-H_2$ compared to the ortho-proton of py additionally supports our theoretical treatment.

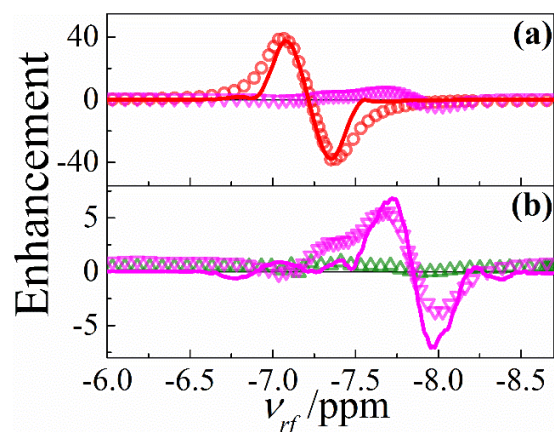


Figure 3S. Dependence of the SABRE-derived NMR enhancement on ν_{rf} at amplitude $\nu_1=20.3$ kHz for different protons. (a) Red: ortho-protons of py, magenta: meta-protons of py, (b) magenta: meta-protons of py, green: para-proton of py. The SABRE effect was observed at the complex of the IrIMes catalyst with py; lines show the simulation results for the 7-spin system IrIMes [H_2 Ir-ePy].

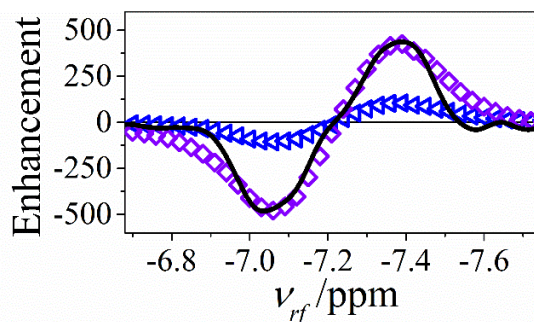


Figure 4S. Dependence of the SABRE-derived NMR enhancement on ν_{rf} at amplitude $\nu_1=20.3$ kHz for H_2 (shown in blue) and $c-H_2$ (shown in violet). The SABRE effect was observed at the complex of the IrIMes catalyst with py; lines show the simulation results for the 7-spin system IrIMes [H_2 Ir-ePy].

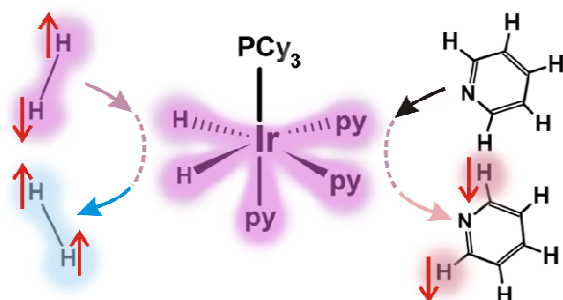
In the case of IrIMes with py we used the NMR parameters of the 7-spin system of IrIMes [H_2 Ir-ePy] (see Table 1S) because the LACs that exist in system IrIMes [H_2 Ir-aPy] occur under different conditions (i.e., at different ν_1 and ν_{rf}). The reason why polarization is transferred directly to ePy, but not to aPy is, most probably, because the J-couplings between $c-H_2$ and protons of ePy are considerably stronger than between $c-H_2$ and aPy. It is also important to mention that, as follows from our 2D NMR experiments, ePy exchanges with free py, which leads to strong polarization of free py.

B. Results for the complex with Crabtree's catalyst

SABRE-induced polarization was also observed for Crabtree's catalyst. The mechanism of the SABRE formation is sketched in Scheme 1S. Experiments were done in the same fashion as in the IrIMes case; again, the SABRE effect is due to spin mixing at LACs in the DTF, as follows from the RF-frequency dependence of polarization. The resulting spectra are shown in Figure 5S. The frequency dependences for the ortho-protons of py are shown in Figure 6S, which acquire the highest NMR enhancement. In all cases the dependence has a positive and a negative component, due to specific LACs in the DTF. As for the IrIMes case, our theoretical treatment reproduces well the experimentally observed dependences.

In Figure 6S, we also demonstrate the dependence on the RF-field amplitude: it is clearly seen that sufficiently high ν_1 values are required to enable the high-field SABRE effect. In contrast to IrIMes, for Crabtree's catalyst the experimental results demonstrate that polarization transfer proceeds from $c-H_2$ to both, ePy and aPy. It can be seen by comparing the ν_{rf} -dependences of the ortho-protons in case of py in the complex with IrIMes (Figures 2S and 3S) and with Crabtree's catalyst (Figure 6S). In the case of IrIMes the frequency dependences are symmetric; also (as we mentioned above) polarization is transferred mainly to ePy. In the case of Crabtree's catalyst the frequency dependences are not symmetric. For this reason, we suggest that polarization is transferred to both ePy and aPy. Hence, we calculated polarization transfer for two channels,

namely for both 8-spin systems of the complexes with Crabtree's catalyst, $[\text{H}_2\text{Ir-aPy}]$ and $[\text{H}_2\text{Ir-ePy}]$; the resulting frequency dependences were added with different weight. Taking into account contributions from the two systems is required to model the experimental curves. Results presented in Figure 6S show that polarization transfer to aPy and ePy is comparable only at low ν_1 , whereas at high ν_1 polarization is mainly transferred to ePy.



Scheme 1S. SABRE formation in the complex of Crabtree's catalyst with parahydrogen and pyridine (py); here PCy_3 stands for tricyclohexyl phosphine. Transfer of the initial singlet spin order (represented by anti-parallel arrows) of the parahydrogen molecule entering the complex results in polarization of py (represented by "down" arrows); also the H_2 molecule goes to its ortho-state (shown by "up" arrows). Here we also indicate that py ligands in axial and equatorial positions can be exchanged and polarized.

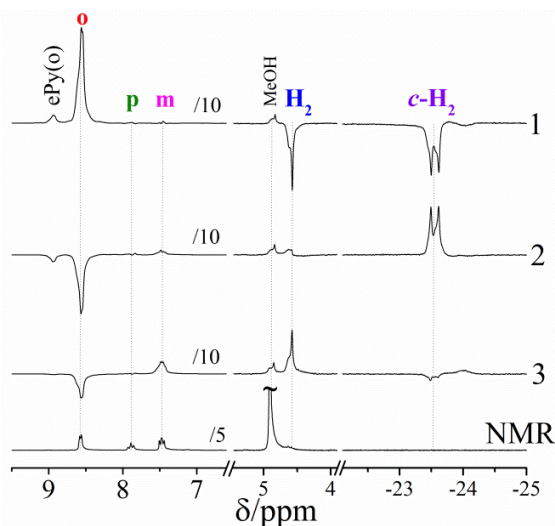


Figure 5S. ^1H RF-SABRE spectra obtained with Crabtree's catalyst after applying an RF-field with amplitude of 28.6 kHz and frequency positions at -7.15 ppm (trace 1), -7.50 ppm (trace 2) and -7.90 ppm (trace 3). The thermal single-scan NMR spectrum is also shown for comparison (bottom trace). Positions of different protons are assigned. Letters *o*, *p*, *m* denote the ortho, para and meta-protons of py; H_2 and *c*- H_2 denote dihydrogen in the bulk and in the catalyst.

Figure 7S presents the results for *c*- H_2 and H_2 . Here the frequency dependences have opposite sign as compared to

the ortho-protons of py (see Figure 6S). Again, to explain the frequency dependences it is necessary to take into account both transfer channels with aPy and with ePy. However, it is not yet clear why the polarization dependences for *c*- H_2 and H_2 are different because one would expect that they are identical as in case of IrIMes (see Figure 4S). The simulation curves for *c*- H_2 and H_2 are sums of those for two channels with aPy and with ePy; the weighting coefficients are different for *c*- H_2 and H_2 . As it is seen from the experimental curves *c*- H_2 behaves here more like *c*- H_2 in the complex with ePy and H_2 more like *c*- H_2 in the complex with aPy.

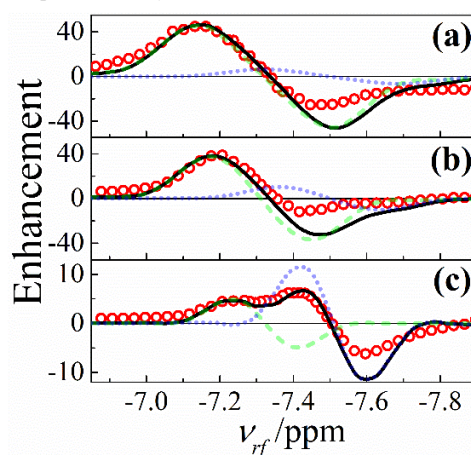


Figure 6S. Dependence of NMR enhancement induced by RF-SABRE on ν_{rf} for different ν_1 values for the ortho-protons of pPy: 28.6 kHz (a), 20.3 kHz (b) and 11.4 kHz (c). Here, the RF-SABRE effects were observed for py with Crabtree's catalyst; lines show the simulation results: dashed green lines – calculation for the 8-spin system Crabtree $[\text{H}_2\text{PIr-ePy}]$, dotted blue lines – calculation for the system Crabtree $[\text{H}_2\text{PIr-aPy}]$, solid black line – sum of the curves given by the dashed and dotted lines.

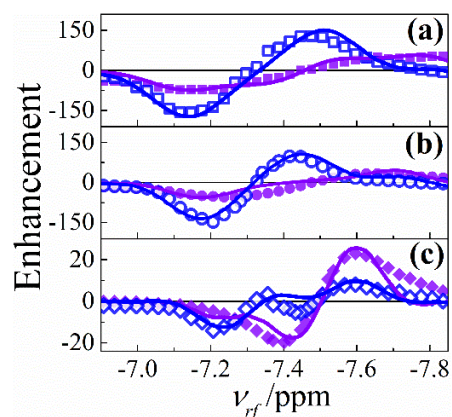


Figure 7S. Dependence of the SABRE-derived NMR enhancement of H_2 on ν_{rf} for different ν_1 values: 28.6 kHz (a), 20.3 kHz (b) and 11.4 kHz (c). The SABRE effect was observed for the complex of Crabtree's catalyst with py; polarization of *c*- H_2 is shown with open blue symbols and that of H_2 is shown with full violet symbols; blue and violet lines show the simulation results for *c*- H_2 and H_2 (see text).

In general, for all the protons under study the experimental results are in good agreement with the simulation. The characteristic dependence of polarization amplitude and its sign on the RF-frequency shows that the reported high-field SABRE effect is due to LACs, which enable efficient and fast transfer of spin order from parahydrogen to the substrate.

C. Results for other substrates

Here it is also of interest to present in more detail the results obtained for other substrates in order to show that the method is not limited to a single chemical system. Figures 8S-13S show the RF-SABRE spectra and RF-SABRE dependences on ν_{rf} for 4,4'-bipyridine, 2,2'-bipyrazine and 3-methyl-1H-pyrazole.

Also for 4,4'-bipyridine or negative RF-SABRE enhancement can be observed by varying the RF-frequency, see Figure 8S. The frequency dependence has the characteristic bimodal shape; polarization for both forms of H₂ always has the phase opposite to that of the substrates, see Figure 9S. The highest RF-SABRE polarization of a substrate proton is 13.

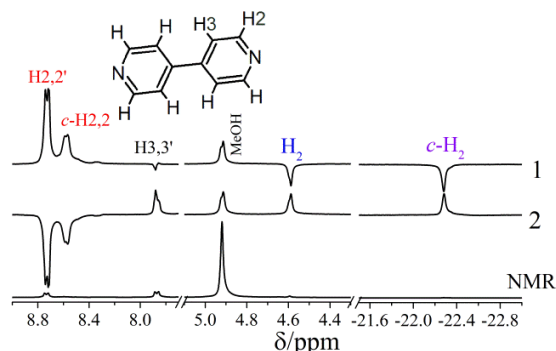


Figure 8S. ¹H RF-SABRE spectra of 4,4'-bipyridine obtained with the IrMes catalyst after applying an RF-field with amplitude of 28.6 kHz and frequency ν_{rf} of -6.6 ppm (trace 1) and -7.60 ppm (trace 2). The thermal single-scan NMR spectrum is also shown for comparison (bottom trace). Positions of different protons are assigned.

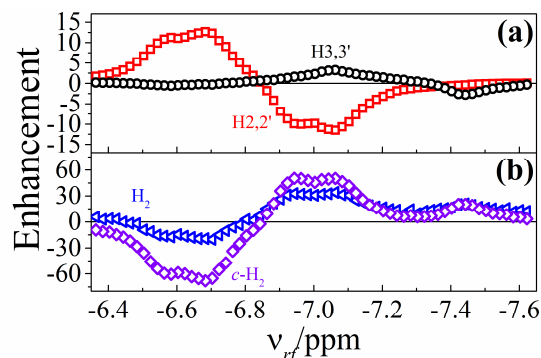


Figure 9S. Dependence of the RF-SABRE effect on ν_{rf} for 4,4'-bipyridine. In (a) the results are shown for the substrate protons and in (b) the results are shown for H₂ and c-H₂. Here $\nu_1=28.6$ kHz; in (a) $\tau_{rf}=10$ s in (b) $\tau_{rf}=0.6$ s.

Considerably higher enhancement is found for 2,2'-bipyrazine, see spectra in Figure 10S. The highest signal enhancement is about 200 (for the H3 proton); for the other two protons the maximal enhancement is about 60. The RF-frequency dependence of polarization is shown in Figure 11S. As previously, the dependence has positive and negative components; one should note that the shape of the dependence is relatively complex due to the larger number of protons involved, thus leading to a spin system of higher complexity.

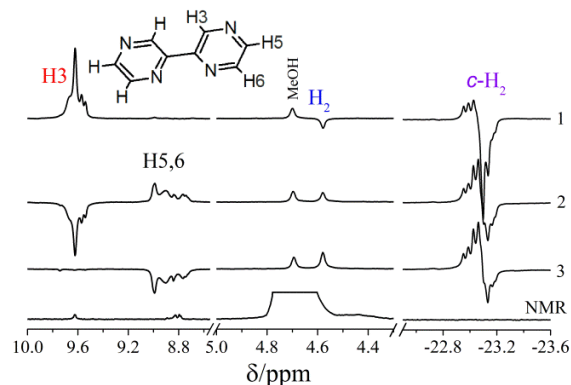


Figure 10S. ¹H RF-SABRE spectra of 2,2'-bipyrazine obtained with the IrMes catalyst after applying an RF-field with amplitude of 28.6 kHz and frequency ν_{rf} of -6.46 ppm (trace 1), -6.84 ppm (trace 2) and -7.18 ppm (trace 3). The thermal single-scan NMR spectrum is also shown for comparison (bottom trace). Positions of different protons are assigned.

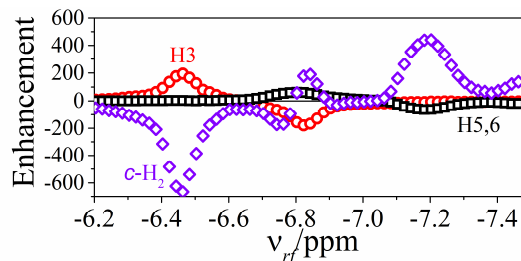


Figure 11S. Dependence of the RF-SABRE effect on ν_{rf} for 2,2'-bipyridine. Here $\nu_1=28.6$ kHz, $\tau_{rf}=0.4$ s.

Finally, let us present the results for 3-methyl-1H-pyrazole. The RF-SABRE effect can be obtained for this compound as well, the characteristic RF-SABRE spectra are given in Figure 12S. Signal enhancements of about 40 are achievable for this substrate; as previously, the RF-SABRE effect can be optimized by setting the RF-frequency and fulfilling the LAC conditions as follows from Figure 13S.

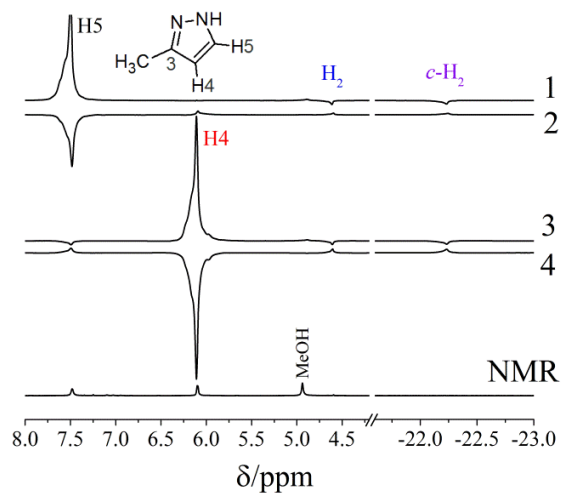


Figure 12S. ^1H RF-SABRE spectra of 3-methyl-1H-pyrazile obtained with the IrImes catalyst after applying an RF-field with amplitude of 28.6 kHz and frequency ν_{rf} of -8.33 ppm (trace 1), -7.93 ppm (trace 2), -7.5 ppm (trace 3) and -7.13 ppm (trace 4). The thermal single-scan NMR spectrum is also shown for comparison (bottom trace). Positions of different protons are assigned.

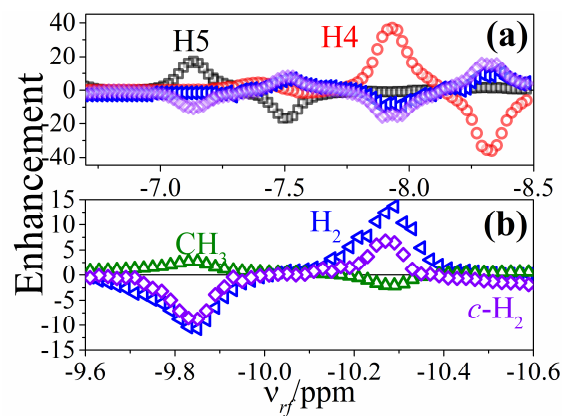


Figure 13S. Dependence of the RF-SABRE effect on ν_{rf} for 3-methyl-1H-pyrazile. In (a) the results are shown for the substrate protons and in (b) for H_2 and $c\text{-H}_2$ and the methyl group of the substrate. Here $\nu_1=28.6$ kHz; in (a) $\tau_{rf}=7$ s in (b) $\tau_{rf}=2.2$ s.

Table 1S. NMR parameters of the spin systems under study.

$J_{\alpha\beta}/\text{Hz}$	$c\text{-H}^1$	$c\text{-H}^2$	Ortho1	Ortho2	Meta1	Meta2	Para
$c\text{-H}^1$	-	-	-	-	-	-	-
$c\text{-H}^2$	-7	-	-	-	-	-	-
Ortho1	3	0.3	-	-	-	-	-
Ortho2	1	1	-0.11	-	-	-	-
Meta1	0.3	0	4.98	0.97	-	-	-
Meta2	0.9	0.6	0.97	4.98	1.41	-	-
Para	0	0	1.79	1.79	7.66	7.66	-
P (only in Crabtree complexes)	23.4	23.4	1	2	0.4	0.6	0
δ_α/ppm	$c\text{-H}_2$		Ortho	Meta	Para		
Crabtree [$\text{H}_2\text{PIr-aPy}$]	-23.4		8.682	7.357	7.969		
Crabtree [$\text{H}_2\text{PIr-ePy}$]	-23.4		9.00	7.565	8.067		
Crabtree [fPy]	-----		8.626	7.532	7.947		
IrIMes [$\text{H}_2\text{Ir-aPy}$]	-22.8		8.064	6.984	7.677		
IrIMes [$\text{H}_2\text{Ir-ePy}$]	-22.8		8.355	7.126	7.775		
IrIMes [f-Py]	-----		8.56	7.466	7.881		

References

- (1) Pravdivtsev, A. N.; Yurkovskaya, A. V.; Vieth, H.-M.; Ivanov, K. L.; Kaptein, R. *ChemPhysChem* **2013**, *14*, 3327.
- (2) Franzoni, M. B.; Graafen, D.; Buljubasich, L.; Schreiber, L. M.; Spiess, H. W.; Münnemann, K. *Phys. Chem. Chem. Phys.* **2013**, *15*, 17233.
- (3) Pravdivtsev, A. N.; Yurkovskaya, A. V.; Lukzen, N. N.; Vieth, H.-M.; Ivanov, K. L. *Phys. Chem. Chem. Phys.* **2014**, *16*, 18707
- (4) Buljubasich, L.; Franzoni, M. B.; Spiess, H. W.; Münnemann, K. *J. Magn. Reson.* **2012**, *219*, 33.